Silicon Core Fibers for Nonlinear Photonics: Applications and Emerging Trends

Meng Huang, Dong Wu, Haonan Ren, Li Shen, and Anna C. Peacock, *Fellow, IEEE*

(Invited Paper)

***Abstract*— Over the past two decades silicon core fibers (SCF) have emerged as a promising platform for use in nonlinear photonic applications. By harnessing the unique optical properties of the crystalline silicon core directly within the fiber geometry, it is possible to imagine compact and low power nonlinear systems that are immediately compatible with existing fiber infrastructures. This paper reviews the recent advances in the development and application of SCFs for nonlinear optical processing and source generation. Particular focus will be placed on novel device designs that benefit from the fiber geometry and post-processing procedures that facilitate integration with existing components.**

***Index Terms*— Lasers and electro-optics, fiber optics, fiber nonlinear optics.**

I. Introduction

NONLINEAR fiber optics has long been a vibrant research area, largely thanks to the invention of low-loss silica fibers in the 1970s [1, 2]. The ability to maintain high optical intensities over long fiber lengths allows nonlinear effects to be observed at much lower power levels than that in bulk materials [3]. However, the extended fiber lengths can be cumbersome, and the narrow near-infrared transmission window of silica glass also limits the operation wavelength range for the nonlinear systems. Over the past two decades, a new class of optical fiber has emerged as a solution to enable more compact nonlinear fiber systems whereby the silica glass core is replaced with a crystalline semiconductor material. As most of the semiconductor materials, including silicon, germanium, zinc selenide, and gallium arsenide, have much stronger nonlinear coefficients and larger transmission windows than silica glass, these crystalline core fibers offer the potential to develop compact and low power systems that extend into wavelength regions that are less accessible for conventional all-silica fibers [4, 5]. Among these in-fiber semiconductor materials, silicon has attracted the most attention both due to its interesting optoelectronic properties, but also as it is well suited to production methods that use traditional silica glass claddings [6, 7].

Silicon core fibers (SCFs) offer the unique potential to combine aspects of traditional integrated silicon photonic systems with optical fiber infrastructures. Notably, these high index contrast waveguides preserve the high confinement and nonlinear parameters available in the planar silicon structures [8], whilst benefiting from the fiber fabrication methods that yield waveguides with circularly symmetric cores, smooth interfaces, and long lengths [9]. Since their first introduction in 2006, SCFs have undergone significant advancement to reduce the transmission losses, enabling them to become established platforms for nonlinear optical applications [10]. SCFs are now predominantly produced using fiber drawing, resulting in the rapid production of waveguides over lengths of several hundreds of meters to ensure low costs and high yields [11]. Moreover, as the fibers are clad in silica, they are also robust and flexible, and thus are compatible with many traditional post-processing procedures, such as fiber tapering and splicing, which can be used to adjust the core dimensions from a few microns down to hundreds of nanometers [12, 13]. As well as providing a means to optimize the properties of the SCFs for different nonlinear applications across various wavelength regions, the post-processing facilitates direct integration with existing fiber components and infrastructures [14].

In this paper, we review efforts to advance the application of the SCFs in nonlinear photonics through their design and optimization. Particular focus will be placed on exploiting the post-processing procedures to enhance the nonlinear performance of the fibers and the resulting systems. Results will be presented over a range of wavelengths extending from the telecom band up to the mid-infrared, highlighting the potential versatility of this platform for applications spanning communications to sensing and healthcare.

II. Fabrication and Post-processing

The first SCF was fabricated by depositing silicon into the

Manuscript received xx xx, xxxx; revised xx xx, xxxx; accepted xx xx, xxxx. Date of publication xx xx, xxxx; date of current version xx xx, xxxx. The data that support the findings of this study are available from the corresponding author upon reasonable request. *(Corresponding authors: Meng Huang & Anna C. Peacock).*

Meng Huang (Meng.Huang@soton.ac.uk), Dong Wu and Anna C. Peacock (acp@orc.soton.ac.uk) are with the Optoelectronic Research Centre, University of Southampton, SO17 1BJ, UK.

Haonan Ren is with the School of Optoelectronic Engineering and instrumentation Science, Dalian University of Technology, Dalian, 116024, China.

Li Shen is with the Wuhan National Laboratory for Optoelectronics, Huazhong University of Science and Technology, Wuhan, 430074, China.

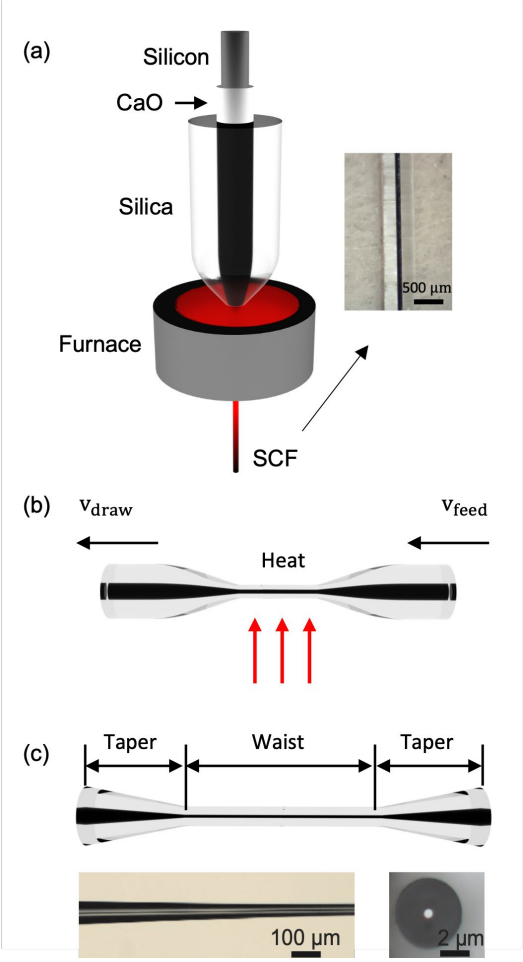

Fig. 1(a) Schematic of the MCD fabrication process and the image of as-drawn SCF. (b) Schematic showing the tapering process to control the crystallinity and dimensions of the silicon core. (c) Schematic of a tapered fiber design optimized for efficient free-space coupling and the images of facets and tapering region for a tapered SCF.

pores of a capillary tube with a high-pressure chemical vapor deposition technique [15]. Although this method can produce SCFs with silicon cores in either a crystalline or amorphous phase, the deposition process is time-consuming, and the fiber lengths are typically limited to a few centimeters. In recent years, the molten core drawing (MCD) method has become the primary fabrication approach for SCFs as it allows for more practical lengths and production times [9]. The procedure begins by sleeving a silicon rod inside a glass tube that has been coated with an interface modifier layer such as calcium oxide (CaO) to create a millimeter-sized preform. The preform is then heated and drawn down into a fiber with micrometer dimensions using a conventional drawing tower, as depicted in Fig. 1(a) [16]. The role of the interface layer is to reduce oxygen contamination from the core during the high temperature drawing, which helps to avoid oxidation of the silicon to silica and reduce defect formation. The modifier also helps to mitigate the expansion mismatch between the core/cladding materials that can lead to residual strain and cracking of the core. The resulting as-drawn SCFs have a poly-silicon core with typical transmission losses in the region of 5-11 dB/cm. The high transmission losses are mainly attributed to small defects and difficulties in controlling the grain growth within the core during the dynamic fiber drawing. Thus, to further improve the transmission of the as-drawn fibers, a tapering procedure has been developed to melt and re-grow the crystalline core to increase the grain sizes, as shown in Fig. 1(b) [17, 18]. As well as reducing the transmission losses down to levels that are comparable with on-chip technologies, this approach has the added advantage of providing a route to tailor the core diameter, which is important for enhancing the nonlinear processes via dispersion engineering [19]. Moreover, by using the tapering to control the longitudinal dimensions of the fiber as illustrated in Fig. 1(c), it is also possible to enhance the coupling efficiency via the taper transition regions. By keeping these transitions short, their contribution to the nonlinear propagation is minimal, so that the SCF performance is still ultimately determined by the waist region. Significantly, through use of these tapering methods, SCFs can now be consistently produced with transmission losses ≤ 1 dB/cm for core sizes ranging from sub-micron (~700 nm) up to a few microns in diameter, over wavelength regions that extend from the telecom band up to 3 µm and beyond [20, 21].

It is worth noting that beyond SCFs, a variety of fibers with alternative crystalline semiconductor core materials have also been fabricated and studied, including germanium [22], silicon-germanium [23], indium antimonide [24], gallium antimonide [25, 26], gallium arsenide [27], zinc selenide and indium phosphide [28]. Interestingly, by offering access to different transmission windows and, in some cases, second order nonlinear processes, these alternative core materials could greatly expand the application potential of the semiconductor fiber platform, assuming the transmission losses can be optimized to have similar values to the SCFs. Moreover, inspired by the remarkable achievements of the planar silicon waveguides devices (i.e., modulators [29], Raman lasers [30-33], and detectors [34, 35]), more complex fiber structures such as p-n junctions [36] and metal/Si systems [37] have also been fabricated with the materials entirely incorporated within the glass cladding, extending the opportunities for all-fiber optoelectronic systems. Beyond this, there is also potential to advance the device performance via integration with more exotic materials including two-dimensional materials and nanostructures [38, 39] by taking advantage of mature side polishing techniques [40], highlighting the versatility of this platform.

III. Nonlinear Demonstrations

A. Wavelength Conversion in the Telecom Band

The early work to demonstrate nonlinear processing using the SCFs focused on nonlinear wavelength conversion via four-wave mixing (FWM). Here, the tapering procedures were used to tailor the SCF core diameters and thus engineer the dispersion profiles to achieve the phase-matching conditions needed for efficient FWM. Due to the ready accessibility of telecom band optical components, the initial research focused on this region. Fig. 2(a) shows a contour map of the group velocity dispersion (GVD, β_2) parameter calculated via the

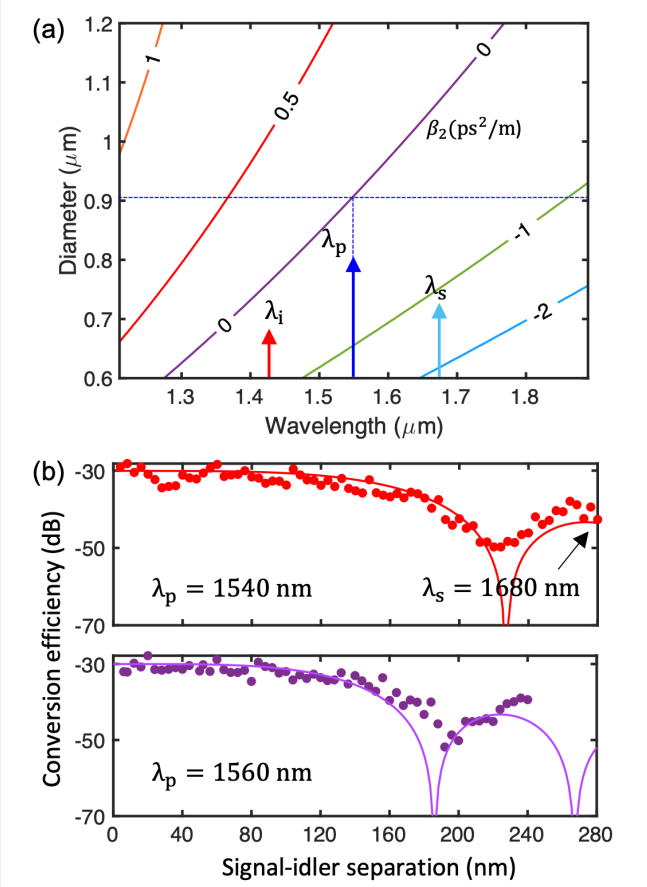

Fig. 2(a) Contour map of the GVD parameter β_2 (ps^2/m) as a function of the SCF core diameter and wavelength. (b) Measured FWM conversion efficiency (normalized) as a function of signal-idler wavelength separation for an SCF with a core diameter of 850 nm and waist length of 5 mm. Top and bottom plots are for different pump wavelengths, as labeled. Solid lines show the simulation results.

well-known eigenvalue equation, for wavelengths covering the extended telecom bands [3]. To achieve efficient phase-matching, it is desirable to work in the anomalous dispersion region, close to the zero-dispersion wavelength (ZDW) [41]. It can be seen that, owing to the strong normal dispersion of the silicon material, it is necessary to reduce the SCF core dimensions to submicron diameters (< 900 nm) to access the anomalous region when the pump wavelength (λ_p) is around 1550 nm.

Fig. 2(b) highlights some of the results to investigate FWM for wavelength conversion in the telecom band, where a continuous wave (CW) telecom pump is used to convert a weak CW signal beam. Here, the normalized conversion efficiency is plotted as a function of signal-idler wavelength separation (λ_s-λ_i), for two different pump wavelengths. The tapered SCF used in this experiment had a core diameter of ~850 nm with a waist length of 5 mm (total length of 9 mm), corresponding to a GVD of β_2 = -0.117 ps^2/m at 1540 nm and β_2 = -0.18 ps^2/m at 1560 nm. Thanks to the high nonlinearity parameter of the small core SCF, high efficiency (~-30 dB) wavelength conversion could be observed with a low pump power (~40 mW). These measurements are in good agreement with calculations for the wavelength conversion efficiency (solid lines), also shown in Fig. 2(b), confirming the predicted dispersion properties of the core [41]. As expected, the conversion bandwidth for the 1540 nm pump source is larger than for the 1560 nm pump as it is closer to the ZDW, highlighting the importance of having accurate control of the core size. The broadest measured wavelength conversion bandwidth for this SCF is more than 260 nm, covering the entire S-, C-, and L- telecom bands. Notably, when the low-power CW signal is tuned to 1680 nm, which is the maximum tuning range of our source, the converted signal is still very strong. Moreover, as the pump power is much lower than the two-photon absorption (TPA) threshold, the wavelength conversion efficiency can be further increased by increasing the pump power [19].

To investigate the suitability of SCF-based wavelength converters for all-optical signal processing, a tapered SCF was subsequently used to convert a 20 Gb/s quadrature phase-shift keying (QPSK) signal from longer to short wavelengths within the telecom band. As FWM takes place at ultrafast timescales, high-speed amplitude and phase-modulated optical signals can be directly converted to the corresponding idler wavelengths [3] [3]. The CW pump was positioned at 1550 nm and the modulated optical QPSK signals were generated at both 1563 nm (C-band) and 1580 nm (L-band). Fig. 3(a) shows the measured spectra recorded by an optical spectrum analyzer (OSA) at the output of the tapered SCF for the two modulated signals. The recorded back-to-back (B-to-B) and converted

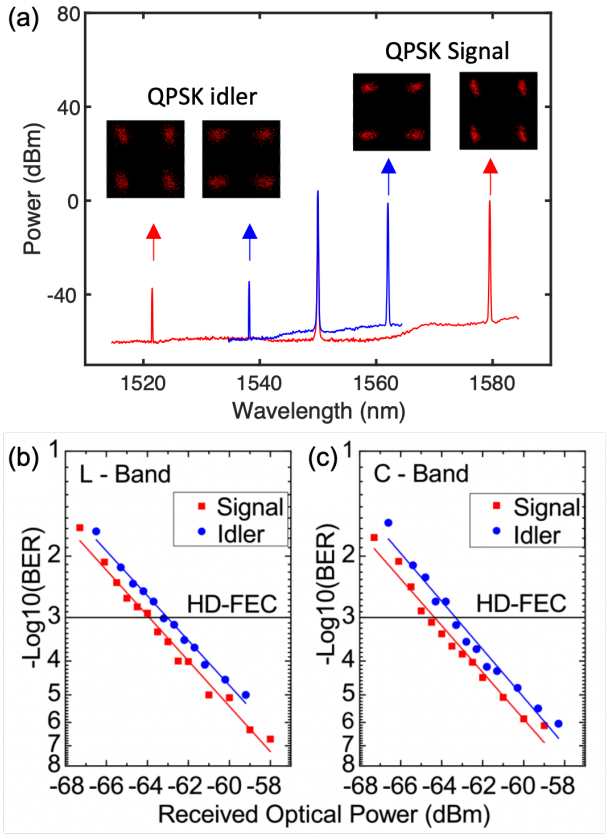

Fig. 3(a) Measured spectra for wavelength conversion of 20 Gb/s QPSK data for two signal wavelengths: 1563 nm and 1580 nm. Insets show the constellation diagrams for the original and converted signals. (b) and (c) show BER curves as functions of the calibrated received power for the 20 Gb/s QPSK data signals in the L-band and C-band, as labeled.

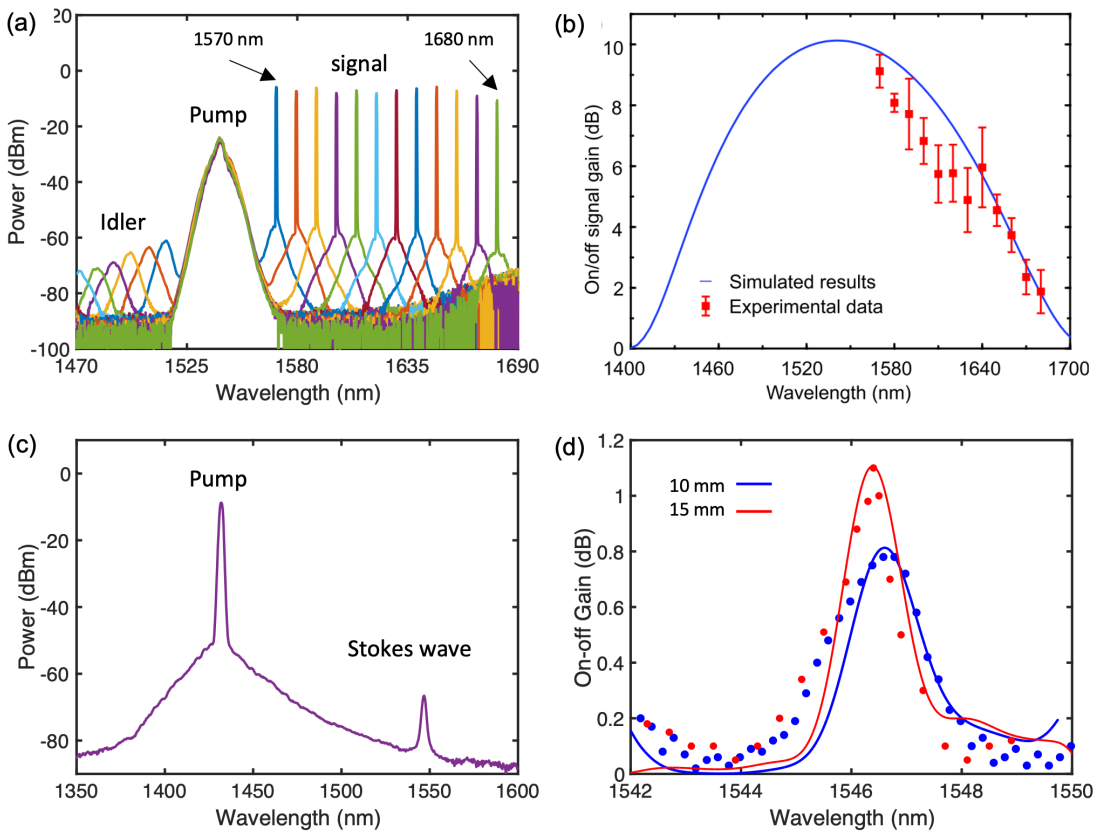

Fig. 4(a) Transmission spectra taken at the output of the SCF as the signal wavelength is tuned from 1570 nm to 1680 nm. (b) Calculated (blue solid line) and measured (red squares) on/off signal gain as a function of signal wavelength, using a pump with ~17 W peak power centered at 1541 nm. (c) Spontaneous Raman emission spectra for the pump wavelength of 1431 nm. (d) Stimulated Raman gains for a 1431 nm pump with a coupled power of 48 mW as measured for various signal wavelengths for SCFs with different lengths, as labeled in the legend.

idler constellation diagrams are also shown as insets. The well-separated constellation diagrams of the converted idler wave indicate that the additional noise introduced by the FWM process is negligible. To better characterize the quality of this SCF-based nonlinear device, Fig. 3(b) and (c) show the measured bit error ratio (BER) as a function of the received power. The conversion has been successfully achieved with a power penalty of 1 to 2 dB at a BER of 3.8×10^{-3} (the hard-decision forward error correction limit) for signals in both the L- and C-bands. These results highlight the robustness of FWM-based SCFs for signal processing in the telecom band.

B. Signal Amplification

In addition to wavelength conversion, amplification is also very important for signal processing systems. The first demonstration of signal amplification using the SCF platform was via a FWM-based optical parametric amplification (OPA) process. To obtain high parametric gain, a short (~670 fs) pulsed laser was used as the pump, positioned at a center wavelength of 1541 nm, whilst a low power (~1 mW) tunable CW source was used as the seed. The SCF used for this experiment was tapered down to a waist diameter of ~915 nm over a length of ~5 mm to optimize the dispersion properties for phase-matching at the pump wavelength. Fig. 4(a) shows the optical spectra generated by the degenerate FWM process, with the signal wavelengths tuned from 1570 nm to 1680 nm. Due to the use of a pulsed pump, the amplified signals and generated idlers occurred as a train of short pulses, as evident from their broad bandwidths measured by the OSA. However, the pump peak power used in this experiment was kept as low as 17 W to avoid gain saturation introduced by the TPA of silicon. By using the duty cycle factor F=1/(40 MHz·670 fs) of the pulsed pump laser, the pulsed peak power of the generated idler and signal beams are extracted by converting the time-averaged power. Then the parametric signal gain was calculated via the signal power with the pump laser on and off. Fig. 4(b) shows the measured signal on/off gain as a function of wavelength. The maximum measured on/off signal gain was ~9 dB at the wavelength of 1570 nm. For the given coupled in pump power, this corresponds to an internal power conversion efficiency (PCE) of ~16 % [42], or an external PCE of ~3 % when taking the coupling loss into consideration. Although these PCEs are comparable to reports in similar planar silicon systems [43], the external efficiency could be further improved up to 10 % if the coupling loss was reduced to ~1 dB per facet by using optimized nano-spike couplers to reduce the reflection between silicon and silica, as described in Section IV [44]. To better understand the relationship between the parametric on/off signal gain and the dispersion properties of SCF, the simulated parametric gain (solid line) is also shown in Fig. 4(b), which was calculated using the dispersion parameters (β_2 ~ 0.042 ps^2/m, β_4 ~ -0.3×10^{-5} ps^4/m) and nonlinear parameter ($\gamma = 40.77$

$W^{-1}\cdot m^{-1}$) estimated for the tapered SCF. The calculated gain curve matches well with the experiment data, again providing evidence that the predicted SCF parameters assuming on a high-crystalline quality silicon core material are accurate.

Raman scattering is another nonlinear effect that can be used to amplify signal waves. Fig. 4(c) shows a spontaneous Raman scattering spectrum obtained with a CW pump at the wavelength of 1431 nm. The Raman emission is around 1550 nm with a bandwidth of ~105 GHz due to the intrinsic 15.6 THz Raman frequency shift and 3.5 ps Raman response time for silicon material. Here, by using the Raman emission, an external signal can be amplified at the expense of pump photons provided it is positioned within the emission bandwidth. Although the Raman bandwidth is narrow for crystalline materials such as silicon, the emission bandwidth could be expanded by using a broadband pump source or even multiple pumps because phase-matching is automatically satisfied through the optical phonons [45]. Fig. 4(d) shows the measured Raman gain for two SCFs with similar core diameters (~900 nm), but different waist lengths (10 mm vs 15 mm), together with simulation results obtained using generalized nonlinear Schrödinger equation (NLSE) [3]. The maximum measured Raman on/off gain was 1.1 dB, obtained in the longer SCF with a CW pump power of only 48 mW. We note that the measured gain was mainly limited by their available pump power and the SCF lengths as the pump power was well below values where nonlinear absorption becomes an issue. Significantly, additional simulations showed that the gain could reach as high as 6 dB by increasing the SCF length to ~10 cm and the power to ~100 mW [20]. However, it is worth noting that as the SCF lengths increase, the linear transmission loss becomes increasingly important. By reducing the losses down to 0.2 dB/cm over a waist length of 6 cm, our recent work has demonstrated peak Raman gains as high as 30.4 dB at wavelengths beyond 2 μm, of interest for gas sensing and spectroscopy [21].

C. Mid-infrared Source Generation

The transmission window of silicon covers wavelengths from 1.1 μm to 8 μm, indicating that the SCF platform has the potential to extend the operation of fiber systems into the mid-infrared (2-20 μm wavelength) regime, which is important for areas such as free-space communications [46], gas sensing [47] and medical diagnostics [48]. Moreover, the dominant nonlinear absorption process of TPA in silicon decreases when using longer wavelengths, particularly beyond the TPA edge of ~2.2 μm, so that the SCF nonlinear performance is expected to be better as we move into the mid-infrared [49]. The only drawback is that the silica cladding has strong absorption beyond 2.5 μm, which could contribute to increased transmission losses in this region. However, by tailoring the cross-sectional geometry of the SCFs to minimize the interaction of the core guided light with the cladding at longer wavelengths, low propagation losses (≤1 dB/cm) are still achievable. Fig. 5(a) shows the estimated linear losses for the fundamental mode of SCFs with different core diameters, as calculated via finite-element method (FEM) simulations for

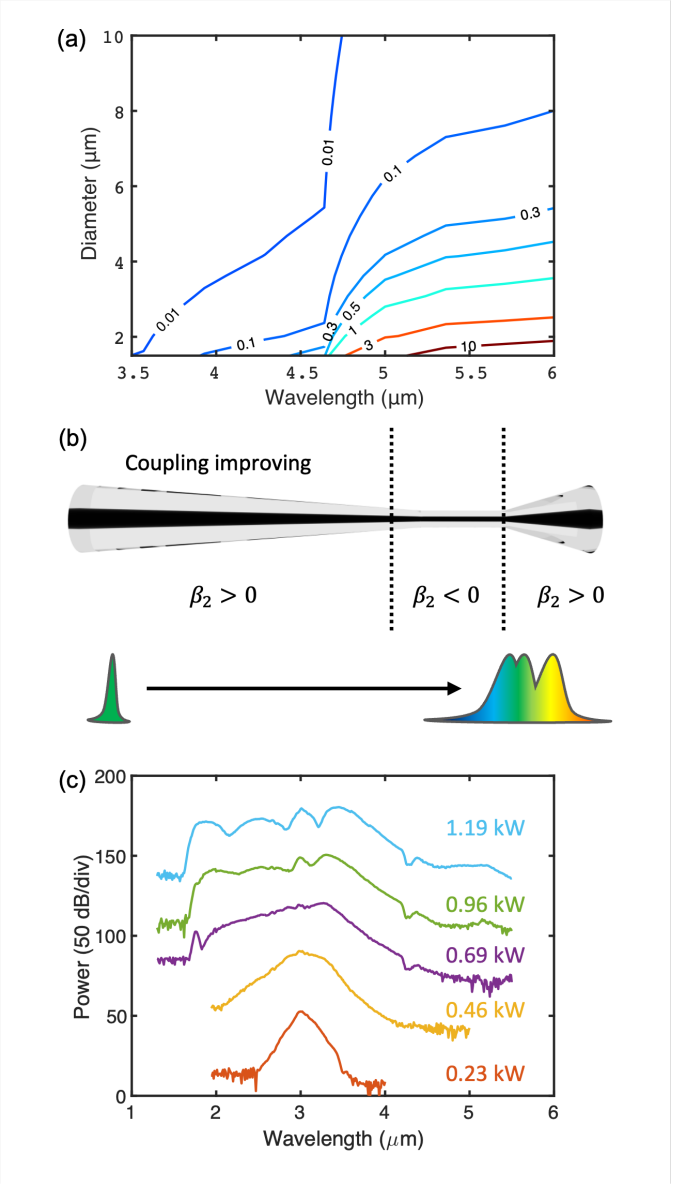

Fig. 5(a) Contour map showing simulated absorption losses for the SCFs in dB/mm as functions of wavelength and fiber core diameter. (b) Schematic of the asymmetric taper design with the different dispersion regions labeled. (c) Experimental spectral broadening as a function of coupled peak input power.

wavelengths beyond 3 μm [50]. By selecting a suitable core diameter, it is clear that low propagation losses (<3 dB/cm) are achievable for wavelengths up to ~5 μm.

To exploit the improved nonlinear performance of the SCFs for wavelengths beyond 2 μm, a mid-infrared supercontinuum generator was designed based on tapered structures. Fig. 5(b) shows the profile of this device. The waist diameter of 2.8 μm was targeted over a short waist length of 1.7 mm to ensure that the 3 μm pump was positioned in the anomalous dispersion region, and that the losses due to interaction with the cladding were minimized. To facilitate maximum coupling into the waist, the input core diameter was slowly tapered down from 10 μm to 2.8 μm over a length of 5.5 mm. At the output, a sharp up-taper (1 mm) was employed to further reduce the interaction with the lossy cladding. By using this fiber profile, self-phase

modulation (SPM) in the initial transition region can act as a seed for efficient FWM and dispersive wave emission, drastically broadening the spectrum at the output. Fig. 5(c) shows the measured supercontinuum spectra obtained with a ~100 fs pulsed pump laser, with coupled average powers increasing from 0.4 mW to 10.8 mW, corresponding to the peak powers given in the legend. The broadest spectrum spans from 1.62 μm to 5.34 μm for a maximum coupled peak power of only 1.19 kW. Thanks to the asymmetric taper design that helped to reduce the interaction of the generated mid-infrared light with the lossy silica cladding, the red edge of the top spectrum was extended well beyond what had been previously achieved in any planar silicon-on-insulator (SOI) waveguide, by around 2 μm. Moreover, the combination of low linear and nonlinear losses resulted in an average usable supercontinuum power of ~6 mW, corresponding to a conversion efficiency as high as ~60 %.

TABLE 1 COMPARISON OF SUPERCONTINUUM GENERATION RESULTS IN SILICON-BASED WAVEGUIDE STRUCTURES.

Platform	Insertion losses (dB)	Pump parameters	Spectral range (μm)	Octaves	Ref.
SOI		100 fs; 18 pJ	1.06-2.4	1.18	[51]
SOI	∗12	70 fs; 16 pJ	1.5-3.3	1.14	[52]
SOI	24.5	70 fs; 2.2 pJ	1.1-2.76	1.33	[53]
SCF	7.6	100 fs; 0.14 nJ	1.62-5.34	1.72	[50]
Suspended SOI	∗15	300 fs; 28.8 nJ	1.2-2.87	1.32	[54]
Si-on-sapphire	20	320 fs; 0.8 nJ	1.9-5.5	1.53	[55]
SiGe-on-Si	12.5	7.5 ps; 0.25 nJ	3.0-8.5	1.5	[56]

∗Values are for the input losses only.

In order to better compare our results with those obtained in other silicon-based waveguide systems, Table 1 provides information of various demonstrations of mid-infrared supercontinuum generation. Although on-chip planar silicon waveguides are still the best choice for applications that require large-scale integration, this comparison shows that SCFs can present an alternative solution for applications where there is a need for efficient and higher power generation of sources that span the near to mid-infrared regions. In particular, thanks to the lower coupling and transmission losses, the SCFs offer a higher conversion efficiency when compared to the other systems represented here, including the large core SiGe platform (conversion efficiency of 48 %) that offers generation of the longest supercontinuum wavelength edge. Moreover, we note that the maximum supercontinuum power and bandwidth generated in the SCF was primarily limited by the available pump, and there is scope to improve the generated output out to wavelengths ~8 μm via access to stronger pumps [48] and optimized fiber coupling methods [50]. Thus, these results highlight the potential benefits of the SCFs over their planar counterparts in terms of power handling and wavelength coverage within the mid-infrared regime.

IV. ALL-FIBER INTEGRATION

As the core diameters of the SCFs used for nonlinear applications are usually much smaller than single-mode fibers (SMFs) (<3 μm verses ~10 μm), it is challenging to realize robust integration of the two fiber types. To solve this problem, we have developed a procedure to produce nano-spike coupling regions onto the ends of the SCFs to facilitate connection with the larger, and lower index, glass cores. This is analogous to the inverse tapers employed by the integrated photonics community, which makes use of the fact that the mode at the nanoscale silicon tip will be predominantly forced into the silica cladding, increasing its size [57, 58]. As well as ensuring efficient mode conversion between the low and high index cores, the inverse tapers also reduce the Fresnel reflection losses. In the case of the SCFs, the inverse nano-spike is produced by tapering the silicon core to a point of collapse, so that a sharp spike appears that connects the coupling facet to the waveguide section, as shown in Fig 6(a). The nano-spike facet is then spliced to a SMF that has been tapered to match the outer diameters of the two fibers, as shown in Fig. 6(b), to further reduce the mode mismatch. A schematic representation of an all-fiber integrated SCF-SMF device is illustrated in Fig. 6(c). For a single coupling facet produced on one end of a SCF, the transmission loss of the waveguide section was measured via a cut-back method to be ~1.7 dB/cm, following which the coupling loss of the spike region could be estimated as < 4 dB [44]. However, additional simulations indicate that the coupling loss could be less than 1 dB by further optimizing the tip geometry and the splicing alignment, thus allowing for efficient all-fiber integration with telecommunication pump and signal sources [44].

Using this all-fiber integration technique, we designed a new SCF-based wavelength convertor, in which the SCF was spliced to a SMF at the input [59]. Thanks to the robust and low loss

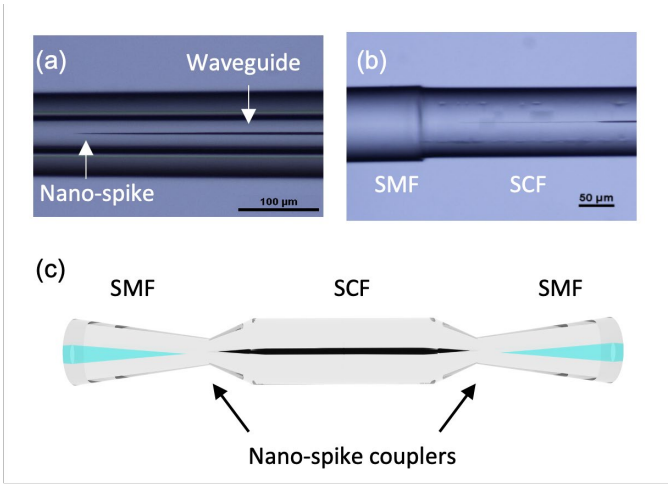

Fig. 6 (a) Microscope image of a nano-spike coupling region. (b) Integrated nano-spike coupled SCF with SMF. (c) Schematic of all-fiber integrated SCF-SMF device.

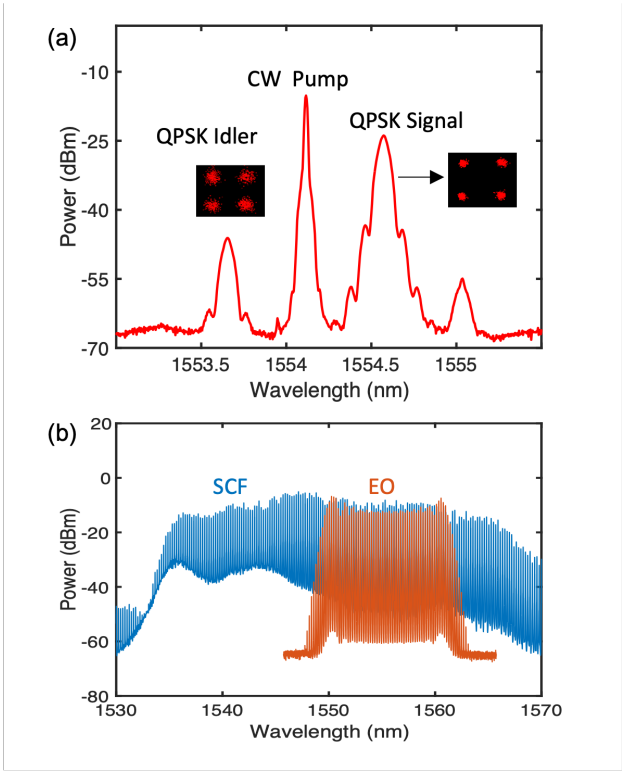

Fig. 7(a) Wavelength conversion of a QPSK data signal, with the signal and idler constellation diagrams shown as insets. (b) Spectral broadening of an electro-optic (EO) frequency comb with 26 GHz line spacing (orange) via a fully fiber integrated SCF nonlinear wave-mixer (blue).

connection, a conversion efficiency as high as -22.1 dB was obtained with a SCF length of only a centimeter, which was a significant improvement over the previous FWM-based wavelength convertor based on free-space coupling. A 20 Gb/s QPSK signal was then used to test the suitability of this device for the construction of ultra-compact, all-fiber-based optical signal processing systems as illustrated by the spectral conversion in Fig. 7(a). Again, the recorded B-to-B and converted idler constellation diagrams are shown as insets, showing that the additional noise from the conversion is low. An optical signal-to-noise ratio (OSNR) penalty of 1 to 2 dB was achieved at the BER of 3.8×10^{-3}, which was comparable with our previous wavelength convertor but with lower pump power (~20 mW vs ~40 mW).

More recently, we have been able to extend our integration methods to produce nano-spike couplers on both ends of the SCF. Although the coupling losses per facet for this system were higher due to difficulties in optimizing the connections at both ends (~8 dB), this device represented the first fully SMF-integrated SCF device suitable nonlinear wave mixing [14]. Specifically, the SCF device was used to broaden an existing telecom band electro-optic comb source (orange spectrum) to expand the number of usable tone lines, as shown by the blue spectrum in Fig. 7(b). Importantly, due to high nonlinearity of the SCF, significant broadening of the bandwidth (from 10 nm to 30 nm) was obtained using only a very short device length (< 2 cm), such that the resulting comb preserved all the key features of the original source including spectral flatness, narrow tone linewidth, high tone power, and low noise levels, as required for applications in telecommunications. Thus, these demonstrations help to highlight the benefits of the SCF platform for exploiting the efficiency of silicon photonics systems, but with the added benefit of all-fiber integration.

V. Conclusion and Outlook

The nonlinear performance of SCFs has been demonstrated in both the telecom band and the mid-infrared region. Most notably, it has been shown that by taking advantage of conventional fiber tapering procedures, it is possible to produce efficient and flexible nonlinear SCF systems. Firstly, high-quality wavelength conversion and amplification were achieved in the telecom band, highlighting the suitability of the SCF platform for use in all-optical signal processing systems. Subsequently, the demonstrations shifted into the mid-infrared region where it was possible to exploit the larger core sizes and low losses of the SCFs for the generation of high power, broadband supercontinuum sources. Finally, integration between the SCFs and SMF via the use of nano-spike couplers was investigated as a route to reduce the coupling losses and improve the robustness of the SCF-based nonlinear devices. Thus, this work highlights the opportunities for SCFs to find use in a wide range of practical all-fiber nonlinear optical systems within application areas that extend beyond those of silica fiber networks to include broadband communications, gas sensing, metrology, and biological imaging [60-62].

Acknowledgment

We would like to acknowledge support from Engineering and Physical Sciences Research Council (EPSRC, EP/P000940/1).

References

[1] K. C. Kao and G. A. Hockham, "Dielectric-fibre surface waveguides for optical frequencies," *Proc. Inst. Electr. Eng.,* Vol. 113, No. 7, pp. 1151-1158, July 1966.
[2] D. Payne and W. A. Gambling. "New silica-based low-loss optical fibre." *Electron. Lett.,* Vol. 10, No. 15, pp. 289-290, July 1974.
[3] G. P. Agrawal, "Nonlinear fiber optics," in *Nonlinear Science at the Dawn of the 21st Century,* pp. 195-211, Dec 2000.
[4] L. Shen *et al.*, "Toward in-fiber nonlinear silicon photonics," *APL Photonics,* Vol. 8, No. 5, May 2023.
[5] T. Schädle and B. Mizaikoff, "Mid-infrared waveguides: a perspective," *Appl. Spectrosc.,* Vol. 70, No. 10, pp. 1625-1638, Oct 2016.
[6] B. Jalali and S. Fathpour, "Silicon photonics," *J. Light. Technol.,* Vol. 24, No. 12, pp. 4600-4615, Dec 2006.
[7] J. Ballato *et al.*, "Silicon optical fiber," *Opt. Express,* Vol. 16, No. 23, pp. 18675-18683, Nov 2008.
[8] J. Leuthold, C. Koos, and W. Freude, "Nonlinear silicon photonics," *Nat. Photonics,* Vol. 4, No. 8, pp. 535-544, Aug 2010.
[9] A. C. Peacock, U. J. Gibson, J. Ballato, "Silicon optical fibres-past, present, and future." *Adv. Phys, X.,* Vol. 1, No. 1, pp. 114-27, Jan 2016.
[10] A. C. Peacock, J. R. Sparks, and N. Healy, "Semiconductor optical fibres: progress and opportunities," *Laser & Photonics Rev.* Vol. 8, No. 1, pp. 53-72. Jan 2014.
[11] A. C. Peacock, "Silicon core fibres for nonlinear photonics: applications and emerging," in *2023 European Conference on Optical Communication (ECOC),* pp. 1-3, Oct 2023.
[12] N. Healy, J. Sparks, P. Sazio, J. Badding, and A. C. Peacock, "Tapered silicon optical fibers," *Opt. Express,* Vol. 18, No. 8, pp. 7596-7601, Apr 2010.
[13] J. H. Chen, Y. T. Sun, and L. A. Wang, "Reducing splicing loss between a silicon-cored optical fiber and a silica optical fiber," *IEEE Photonics Technol. Lett.,* Vol. 28, No. 16, pp. 1774-1777, May 2016.

[14] R. Sohanpal *et al.*, "All-fibre heterogeneously-integrated frequency comb generation using silicon core fibre," *Nat. Commun.,* Vol. 13, No. 1, pp. 3992, Jul 2022.
[15] P. J. Sazio *et al.*, "Microstructured optical fibers as high-pressure microfluidic reactors," *Science*, Vol. 311, No. 5767, pp. 1583-1586, Mar 2006.
[16] E. F. Nordstrand, A. N. Dibbs, A. J. Eraker, and U. J. Gibson, "Alkaline oxide interface modifiers for silicon fiber production," *Opt. Mater. Express*, Vol. 3, No. 5, pp. 651-657, May 2013.
[17] F. H. Suhailin *et al.*, "Tapered polysilicon core fibers for nonlinear photonics," *Opt. Lett.,* Vol. 41, No. 7, pp. 1360-1363, Apr 2016.
[18] Y. Franz *et al.*, "Material properties of tapered crystalline silicon core fibers," *Opt. Mater. Express,* Vol. 7, No. 6, pp. 2055-2061, Jun 2017.
[19] D. Wu *et al.,* "Net optical parametric gain in a submicron silicon core fiber pumped in the telecom band," APL Photonics, Vol. 4, No. 8, Aug 2019.
[20] M. Huang *et al.*, "Continuous-wave Raman amplification in silicon core fibers pumped in the telecom band," *APL Photonics,* Vol. 6, No. 9, Sep 2021.
[21] M. Huang *et al.*, "Raman amplification at 2.2 μm in silicon core fibers with prospects for extended mid-infrared source generation," *Light Sci. Appl.,* Vol. 12, No. 1, pp. 209, Aug 2023.
[22] J. Ballato *et al.,* "Glass-clad single-crystal germanium optical fiber," *Opt. Express,* Vol. 17, No. 10, pp. 8029-8035, May 2009.
[23] D. A. Coucheron *et al.,* "Laser recrystallization and inscription of compositional microstructures in crystalline SiGe-core fibres," Nat. commun., Vol. 7, No. 1, pp. 13265, Oct 2016.
[24] J. Ballato *et al.,* "Binary III-V semiconductor core optical fiber," Opt. Express, Vol. 18, No. 5, pp. 4972-9, Mar 2010.
[25] B. L. Scott and G. R. Pickrell, "Fabrication of GaSb optical fibers," *Processing and Properties of Advanced Ceramics and Composites V: Ceramic Transactions*, Vol. 240, pp. 65, Jul 2013.
[26] S. Song *et al.,* "Crystalline GaSb-core optical fibers with room-temperature photoluminescence," *Opt. Mater. Express,* Vol. 8, No. 6, pp. 1435-40, Jun 2018.
[27] T. Zaengle *et al.,* "A novel route to fibers with incongruent and volatile crystalline semiconductor cores: GaAs," ACS Photonics, Vol. 9, No. 3, pp. 1058-64, Feb 2022.
[28] T. Zaengle, E. Martinez, T. W. Hawkins, C. McMillen, and J. Ballato, "A novel route to fibers with volatile crystalline semiconductor cores Part 2: Selenides and phosphides," *Optical Materials,* Vol. 145, pp. 114388, Nov 2023.
[29] G. T. Reed, G. Mashanovich, F. Y. Gardes, and D. Thomson, "Silicon optical modulators," *Nat. photonics,* Vol. 4, No. 8, pp. 518-526, Aug 2010.
[30] O. Boyraz and B. Jalali, "Demonstration of a silicon Raman laser," *Opt. Express,* Vol. 12, No. 21, pp. 5269-5273, Oct 2004.
[31] H. Rong *et al.,* "A continuous-wave Raman silicon laser," *Nature*, Vol. 433, No. 7027, pp. 725-728, Feb 2005.
[32] H. Rong *et al.,* "An all-silicon Raman laser," *Nature,* Vol. 433, No. 7023, pp. 292-294, Jan 2005.
[33] H. Rong *et al.*, "A cascaded silicon Raman laser," *Nat. Photonics,* Vol. 2, No. 3, pp. 170-174, Mar 2008.
[34] D. Thomson *et al.,* "Optical detection and modulation at 2 μm-2.5 μm in silicon," *Opt. Express,* Vol. 22, No. 9, pp. 10825-10830, May 2014.
[35] J. J. Ackert et al. , "High-speed detection at two micrometres with monolithic silicon photodiodes," *Nat. Photonics,* Vol. 9, No. 6, pp. 393-396, Jun 2015.
[36] D. Homa, A. Cito, G. Pickrell, C. Hill, and B. Scott, "Silicon fiber with pn junction," *Appl. Phys. Lett.,* Vol. 105, No. 12, pp. 105, Sep 2014.
[37] S. Song *et al.,* "Localised structuring of metal-semiconductor cores in silica clad fibres using laser-driven thermal gradients," *Nat. Commun.,* Vol. 13, No. 1, pp. 2680, May 2022.
[38] D. Akinwande *et al.,* "Graphene and two-dimensional materials for silicon technology." *Nature,* Vol. 573, No. 7775, pp. 507-18, Sep 2019.
[39] H. Zhang *et al.,* "Enhanced all-optical modulation in a graphene-coated fibre with low insertion loss." *Sci. Rep,* Vol. 6, No. 1, pp. 23512, Mar 2016.
[40] W. C. Lu *et al.*, "D-shaped silicon-cored fibers as platform to build in-line Schottky photodetectors," *IEEE Photonics Technol. Lett.,* Vol. 33, No. 6, pp. 317-20, Feb 2021.
[41] D. Wu *et al.*, "Four-wave mixing-based wavelength conversion and parametric amplification in submicron silicon core fibers," *IEEE J. Sel. Top. Quantum Electron.,* Vol. 27, No. 2, pp. 1-11, Sep 2020.
[42] A. H. Beshr, "Study of ASE noise power, noise figure and quantum conversion efficiency for wide-band EDFA," *Optik,* Vol. 126, No. 23, pp. 3492-5, Dec 2015.
[43] X. Liu, R. M. Osgood, Y. A. Vlasov, and W. M. Green, "Mid-infrared optical parametric amplifier using silicon nanophotonic," *Nat. Photonics,* Vol. 4, No. 8, pp. 557-60, Aug 2010.
[44] H. Ren *et al.,* "Tapered silicon core fibers with nano-spikes for optical coupling via spliced silica fibers," *Opt. Express,* Vol. 25, No. 20, pp. 24157-24163, Oct 2017.
[45] D. R. Solli, P. Koonath, and B. Jalali, "Broadband Raman amplification in silicon," *Appl. Phys. Lett.,* Vol. 93, No. 19, Nov 2008.
[46] K. Zou *et al.*, "High-capacity free-space optical communications using wavelength-and mode-division-multiplexing in the mid-infrared region," *Nat. Commun.,* Vol. 13, No. 1, pp. 7662, Dec 2022.
[47] U. Willer, M. Saraji, A. Khorsandi, P. Geiser, and W. Schade, "Near-and mid-infrared laser monitoring of industrial processes, environment and security applications," *Opt. Lasers Eng.,* Vol. 44, No. 7, pp. 699-710, Jul 2006.
[48] A. B. Seddon, "Mid-infrared (IR)-A hot topic: The potential for using mid-IR light for non-invasive early detection of skin cancer in vivo," *Phys. Status Solidi B,* Vol. 250, No. 5, pp. 1020-1027, May 2013.
[49] H. Ren *et al.*, "Nonlinear optical properties of polycrystalline silicon core fibers from telecom wavelengths into the mid-infrared spectral region," *Opt. Mater. Express,* Vol. 9, No. 3, pp. 1271-1279, Mar 2019.
[50] H. Ren *et al.*, "Low-loss silicon core fibre platform for mid-infrared nonlinear photonics," *Light Sci. Appl.,* Vol. 8, No.1, pp. 105, Nov 2019.
[51] N. Singh *et al*., "Octave-spanning coherent supercontinuum generation in silicon on insulator from 1.06 μm to beyond 2.4 μm," *Light Sci. Appl.,* Vol. 7, No. 1, pp. 17131, Jun 2018.
[52] B. Kuyken *et al.,* "An octave-spanning mid-infrared frequency comb generated in a silicon nanophotonic wire waveguide," *Nat. commun.,* Vol. 6, No. 1, pp. 6310, Feb 2015.
[53] J. Wei *et al.,* "Supercontinuum generation assisted by wave trapping in dispersion-managed integrated silicon waveguides," *Phys. Rev. Appl.,* Vol. 14, No. 5, pp. 054045, Nov. 2020.
[54] R. Kou *et al.,* "Mid-IR broadband supercontinuum generation from a suspended silicon waveguide," *Opt. Lett.,* Vol. 43, No. 6, pp. 1387-1390, Mar 2018.
[55] N. Singh *et al.,* "Midinfrared supercontinuum generation from 2 to 6 μm in a silicon nanowire," *Optica,* Vol. 2, No. 9, pp. 797-802, Sep 2015.
[56] M. Sinobad *et al.,* "Mid-infrared octave spanning supercontinuum generation to 8.5 μm in silicon-germanium waveguides," *Optica,* Vol. 5, No. 4, pp. 360-366, Apr 2018.
[57] V. R. Almeida, R. R. Panepucci, and M. Lipson, "Nanotaper for compact mode conversion," *Opt. Lett.,* Vol. 28, No. 15, pp. 1302-1304, Aug 2003.
[58] M. Wood, P. Sun, and R. M. Reano, "Compact cantilever couplers for low-loss fiber coupling to silicon photonic integrated circuits," *Opt. Express,* Vol. 20, No. 1, pp. 164-172, Jan 2012.
[59] M. Huang *et al.,* "Fiber integrated wavelength converter based on a silicon core fiber with a nano-spike coupler," *IEEE Photon. Technol. Lett.,* Vol. 31, No. 19, pp. 1561-1564, Aug 2019.
[60] D. Liang, J. E. Bowers,„ "Recent progress in lasers on silicon," *Nat. Photonics.,* Vol. 4, No. 8, pp. 511-7, Aug 2010.
[61] R. Soref, "Mid-infrared photonics in silicon and germanium," *Nat.Photonics,* Vol. 4, No. 8, pp. 495-7, Aug 2010.
[62] L. Zhang, A. M. Agarwal, L. C. Kimerling, J. Michel, "Nonlinear Group IV photonics based on silicon and germanium: from near-infrared to mid-infrared," *Nanophotonics,* Vol. 3, No. 4-5, pp. 247-68, Aug 2014.

Meng Huang was born in Nanchang, Jiangxi province, China in 1994. He received the B.Eng. degree in electronic science and technology from the Harbin Institute of Technology, Harbin, China, in 2016, and the M.Eng. degree in optical engineering from the Huazhong University of Science and Technology, Wuhan, China, in 2019. Since 2019, he has been working toward the Ph.D. degree with the Optoelectronics Research Centre, University of Southampton, Southampton, U.K. His current research interests include nonlinear silicon photonics and semiconductor core fibers.

Dong Wu received the B.Eng. degree in optical information science and technology from Wuhan University, Wuhan, China, in 2014 and the M.Phil. degree in optical engineering from Shandong University, Jinan, China, in 2017. Since then, she has been working toward the Ph.D. degree with the Optoelectronics Research Centre, University of Southampton, Southampton, U.K and received her PhD degree in 2022. Her main research interest is the study of the nonlinear effects in silicon core fibers.

Haonan Ren received the B.Eng. degree in electrical engineering and electronics from the University of Edinburgh, Edinburgh, U.K., and Xiamen University, Xiamen, China, in 2015, and the Ph.D. degree in nonlinear optics from the University of Southampton, Southampton, U.K., in 2019. His current research interests include nonlinear fiber optics and tapered silicon core fibers.

Li Shen received the B.Sc. and M.Phil. degrees from the Huazhong University of Science and Technology, Wuhan, China, in 2009 and 2012, respectively, and the Ph.D. degree from the Optoelectronics Research Centre, University of Southampton, Southampton, U.K., in 2015. He is currently an Associate Professor with HUST, and his research interests include novel semiconductor photonic devices, silicon photonics, and mid-infrared photonics.

Anna C. Peacock (Fellow, IEEE) received the B.Sc. and M.Sc. degrees in physics from the University of Auckland, Auckland, New Zealand, in 1999 and 2001, respectively, and the Ph.D. degree from the Optoelectronics Research Centre (ORC), University of Southampton, Southampton, U.K., in 2004. She is currently a Professor of Photonics within the ORC, University of Southampton. In 2007, she received a five-year Royal Academy of Engineering Research Fellowship, following which she established the Nonlinear Semiconductor Photonics Group, where the focus of the research is on the design and development of novel semiconductor waveguides. She is a Fellow of Optica, the Institute of Electrical and Electronics Engineers, and the Institute of Physics.